

Chapter 14

**METHANE STORAGE IN MICROPOROUS CARBONS –
EFFECT OF POROSITY AND SURFACE CHEMICAL
COMPOSITION TESTED ON
REALISTIC CARBON MODEL**

Artur P. Terzyk^{1,}, Sylwester Furmaniak¹, Radosław P. Wesolowski¹,
Piotr A. Gauden¹, Peter J. F. Harris²*

¹Physicochemistry of Carbon Materials Research Group, Faculty of Chemistry, Nicolas
Copernicus University, 7 Gagarin St., PL 87-100 Toruń, Poland

²Centre for Advanced Microscopy, University of Reading, Whiteknights, Reading RG6
6AF, UK

ABSTRACT

Methane storage in carbon materials is widely studied since activated carbons are still one of the most promising adsorbents applied for this purpose. Many computer simulations performed for carbon models composed of slit-like pores showed that the optimal slit for methane storage has the width in the range 0.7-0.8 nm. However, there are still new reports in the literature showing that the slit-like model of carbon pores is far from reality. For example, based on the observation of HRTEM images Harris et al. proposed the fullerene-like model of “hard” activated carbon. This model was tested in our previous studies and the results showed that many empirical correlations observed for different activated carbons can be successfully recovered by the model. In the presented chapter using the model of Harris the results of GCMC simulations of methane storage are shown. Two sets of data are presented, and the results of the change in carbon porosity and surface chemical composition on methane adsorption are shown. Using the Monte Carlo method the porosity of carbon model was changed and controlled. The

* Corresponding author, e-mail: aterzyk@chem.umk.pl

changes in chemical composition of carbon surface layers were obtained *via* random introduction of carbonyl groups (“virtual oxidation”). Next for all models methane adsorption isotherms were simulated by the standard GCMC method. The results obtained show systematic changes due to porosity as well as the appearance of oxygen on the carbon surface. Moreover it is shown that the parameters of the Dubinin-Astakhov model (as well as the parameter k used for approximation of apparent saturation pressure of methane) as well as the constants of Sips and Toth equations depend on carbon porosity and chemical composition of carbon surface.

1. INTRODUCTION AND THE AIMS OF THE STUDY

Methane storage in carbon materials is widely studied since activated carbons are still the most promising adsorbents applied for this purpose. There are reviews in the literature dealing with this subject [1] and showing the optimal procedures for obtaining carbons, coals and MOFs [2-9] possessing high methane storage capability. The results of computer simulations performed for carbon models composed of slit-like pores showed that the optimal slit for methane storage has a width in the range 0.7-0.8 nm [10,11]. However, there are still new reports in literature showing that the slit-like model of carbon pores is far from reality [12-17]. For example, based on the observation of HRTEM images Harris et al. proposed the fullerene-like model of “hard” activated carbon [18-23] (called later the Virtual Porous Carbon (VPC)). This model was tested in our previous studies and the results showed that many empirical correlations observed during adsorption on different activated carbons can be successfully recovered by the model [24-27]. In the presented chapter using the model of Harris the results of GCMC simulations of methane storage are shown. Simulations offer many possibilities unavailable in experiment namely one can simply manipulate with carbon porosity by adding/deleting new fragments to the structure [24] or by shifting those fragments, the pore size distribution (PSD) curve can be calculated from geometric considerations [25,28] thus the absolute (true) porosity is known [25,28] and what is also important, different functional groups (for example carbonyls) can be added to structure at arbitrarily chosen places and in controlled amounts (using what we call “virtual oxidation”).

An important problem in projecting of carbon adsorbents for optimal methane storage is the application of theoretical models to a description of experimental data. In this field the most popular is the adsorption isotherm equation proposed by Dubinin et al. [29,30]:

$$a(p, T) = a_0(T) \exp \left[- \left(\frac{A(p, T)}{E} \right)^n \right] \quad (1)$$

where a_0 is the adsorption capacity of a given system, E is the characteristic adsorption energy, n is the best fit parameter related to the heterogeneity of an adsorbent, and A is adsorption potential defined as:

$$A(p, T) = RT \ln \frac{p_s^*(T)}{p} \quad (2)$$

where p_s^* is saturated vapour pressure (for subcritical gas) and/or the apparent saturated vapour pressure if adsorption of supercritical gas is measured. Here a problem arises, since many relations have been proposed to evaluate this apparent pressure (see for example [31]). Among those relations the most general was proposed by Amankwah and Schwarz [32]:

$$p_s^*(T) = \left(\frac{T}{T_C} \right)^k p_C \quad (3)$$

where T_C and p_C are the critical temperature and pressure, respectively, and k is the parameter specific for the system studied. In their paper Amankwah and Schwarz showed that for experimental data measured for different activated carbons the value of this parameter changes in the range 2.10-2.73 (methane adsorption) or 2.72-4.16 (hydrogen adsorption). Note that in the case of $k = 2$, Eq. (3) reduces to the relation proposed by Dubinin [33] however this original relation not always leads to the single characteristic curve as pointed out by Ozawa et al. [34].

The adsorption capacity a_0 from Eq.(1) decreases with rising temperature due to thermal expansion of an adsorbate. To take it into account in this chapter the relation proposed by Ozawa et al. [34] is used:

$$a_0(T) = a_0^B \exp[-\alpha(T - T_B)] \quad (4)$$

where a_0^B is the adsorption capacity at the boiling point temperature (T_B) and $\alpha = 0.0025$ 1/K [34].

Other models widely applied in the field of methane adsorption are those proposed by Toth and Sips [35-39] in the following forms [40]:

$$a(p, T) = \frac{a_m(T) \cdot K_T(T) \cdot p}{\left(1 + (K_T(T) \cdot p)^t\right)^{\frac{1}{t}}} \quad (5)$$

$$a(p, T) = \frac{a_m(T) \cdot (K_S(T) \cdot p)^{\frac{1}{n}}}{1 + (K_S(T) \cdot p)^{\frac{1}{n}}} \quad (6)$$

where a_m is the maximum adsorption value, K_T and K_S are constants specific for adsorbate - adsorbent pairs, t and n (also specific studied system) are related to the heterogeneity [40]. In Toth equation t is a parameter which is usually less than unity. When $t = 1$, the Toth isotherm

reduces to the famous Langmuir equation; hence like in the Sips equation the parameter n is said to characterize the system heterogeneity. If it is deviated further away from unity, the system is said to be more heterogeneous. The parameter n of the Sips equation is usually greater than unity and therefore, the larger is the parameter the more heterogeneous is the system. As pointed out by Do [40] the behaviour of Sips equation is the same as that of the Freundlich equation except that the Sips equation possesses a finite saturation limit when the pressure is sufficiently high. However, it still shares the same disadvantage with the Freundlich isotherm in that neither of them have the right behaviour at low pressure, that is they do not give the correct Henry law limit. Contrary, the Toth equation has correct limits when p approaches either zero or infinity.

Taking into account the temperature dependence of the parameters, following Do [40]:

$$K_T(T) = K_{T,0} \exp\left[\frac{Q_T}{RT}\right] \quad (7)$$

$$K_S(T) = K_{S,0} \exp\left[\frac{Q_S}{RT}\right] \quad (8)$$

where $K_{T,0}$ and $K_{S,0}$ are almost temperature independent entropic factors, Q_T and Q_S are the enthalpy values related to each constant. Do [40] proposed the following equations for temperature dependence of t (Toth Eq.(5)) and n (Sips Eq.(6)) parameters:

$$t = t_0 + \chi \left(1 - \frac{T_0}{T}\right) \quad (9)$$

$$\frac{1}{n} = \frac{1}{n_0} + \chi \left(1 - \frac{T_0}{T}\right) \quad (10)$$

where t_0 and n_0 are the values of parameters at some reference temperature (T_0), and χ is the proportionality factor. In this chapter the reference temperature as equal to 268 K is assumed. Also the value of maximum adsorption is temperature dependent due to the thermal expansion of adsorbed molecules. For this case one can assume the temperature dependence of a_m analogous as in Eq. (4):

$$a_m(T) = a_m^B \exp[-\alpha(T - T_B)] \quad (11)$$

The major purpose of this chapter is to check to what extent changes in porosity and in the chemical composition of activated carbon change the parameters of Eqs.(1) (5) and (6). Special attention is also paid to the parameter k of Eq.(3) since it is empirical. To check this we use the VPC model proposed by Harris et al. and the GCMC simulations of supercritical methane adsorption.

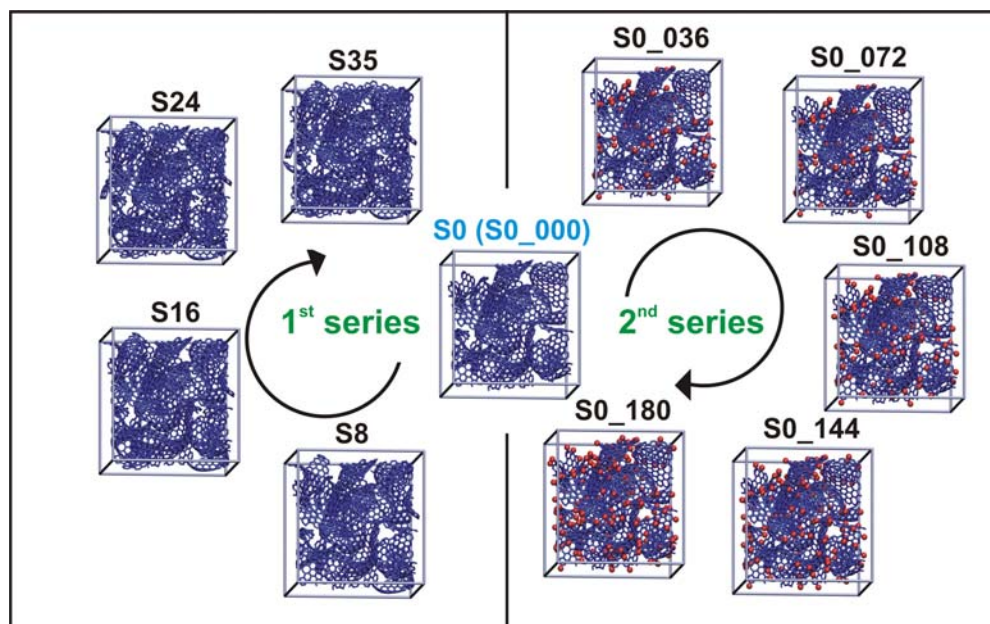


Figure 1. Schematic representation of the construction of VPCs applied in this chapter. From the initial structure called S0 (or S0_000) the structures with gradually changed porosity (1st series - shown on LHS) or contents of surface carbonyls (2nd series - RHS) are obtained.

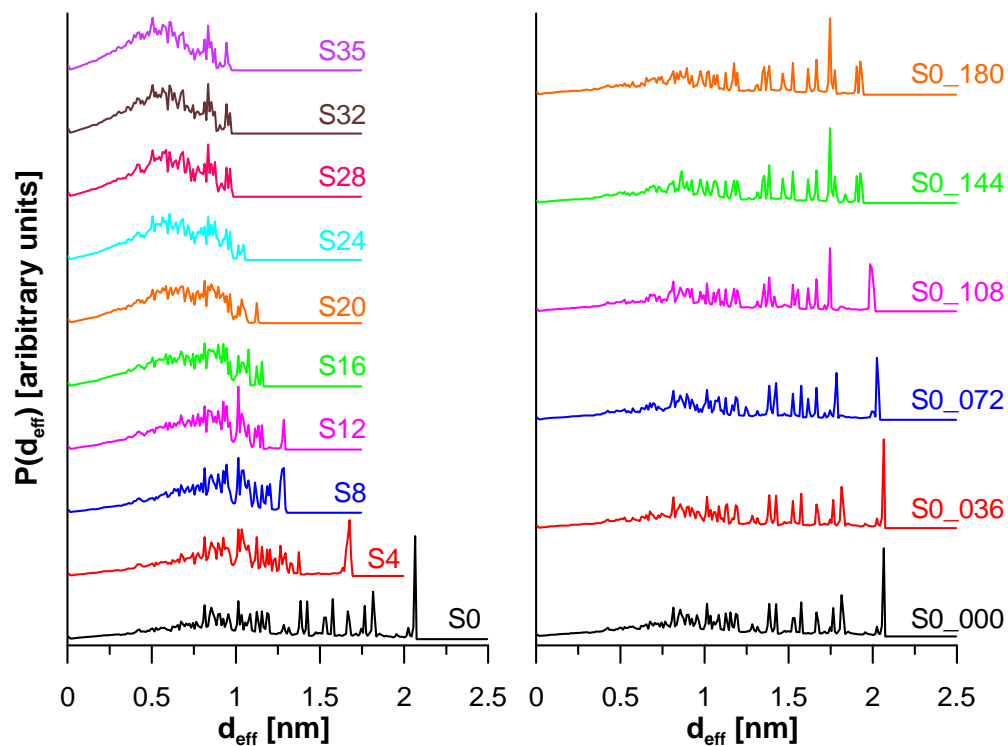


Figure 2. Histogram of the pore diameters for studied VPCs.

2. VIRTUAL POROUS CARBONS

Two series of VPCs generated previously [24,27] and based on the model proposed by Harris [18,19,21] are studied. As was shown previously application of those models leads to successful recovering of many empirical relations obtained in real systems [24-27]. The initial structure called S0 is described in details previously [24]. The first series of VPCs (having systematic changes in porosity) was generated by the Monte Carlo insertion of carbon fragments in the pores of S0 structure using the method described in details previously (see Figure 1) [24]. Those structures are labeled as: S0, S4, S8, S12, S16, S20, S24, S28, S32 and S35. The second series was obtained by introduction of surface carbonyl groups using described recently so called “virtual oxidation” procedure [27]. Obtained structures are labeled as S0_000 (initial structure - identical with S0), S0_036, S0_072, S0_108, S0_144 and S0_180, where the last number denotes the number of introduced carbonyl surface groups. All structures were placed in cuboidal simulation box having dimensions $4.6 \times 4.6 \times 4.6$ nm.

The porosity of studied structures was determined by the geometric method proposed by Bhattacharya and Gubbins [28]. This method leads to the pore size distribution function of any structure placed in a simulation box. In this method a uniform grid of points is generated in the simulation box (for studied structures $100 \times 100 \times 100$) and for each such a point (located in pore) the largest sphere containing this point (and situated in the pore) is found. The diameter of this sphere is equal to the diameter of the pore and the collection of histogram of the diameters of pores for each such a point of the grid makes it possible to plot the histogram of the pore diameters (related to the PSD curve). The program works in an iterative way. For each node of the grid located in the structure of carbon, the centre of the testing sphere is placed randomly (at the start as the centre of the sphere the coordinates of the node are assumed, the diameter of the sphere is limited by the distance to the nearest fragment of carbon structure). Each displacement of the centre of the sphere (the sphere must contain the test point) leading to a rise in the diameter is accepted and the next attempts of displacement are made. The program stops calculations for a given point when after 1000 following iterations a sphere with a larger diameter is not found. The histogram of dimensions of spheres for all nodes is equivalent to the histogram of pore dimensions [24-27]. Figure 2 shows the results for all studied structures.

3. INTERMOLECULAR INTERACTIONS

Methane molecules were modelled using the rigid 5-centre model [41]. In this model each atom of methane molecule is approached by a single Lennard-Jones site with a single charge. Generally the energy of interactions between a pair of molecules can be written as:

$$U(\mathbf{r}) = \sum_{i=1}^5 \sum_{j=1}^5 U_{LJ}^{ij}(\mathbf{r}_{ij}) + U_{electr}(\mathbf{r}) \quad (12)$$

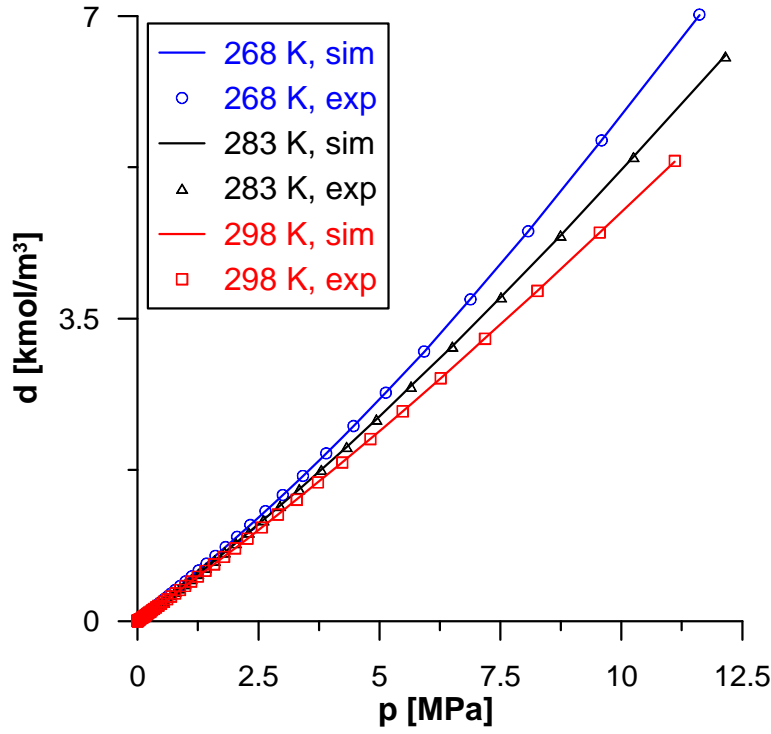


Figure 3. The comparison of bulk methane densities obtained from GCMC using the parameters from this chapter with the densities from experiment [55].

where r is the distance between the centres of molecules (this energy depends also on angular orientation of molecules), $U_{LJ}^{ij}(r_{ij})$ is the energy of dispersion interactions between a pair of centres i and j being placed at the distance r_{ij} , and calculated from the truncated LJ potential:

$$U_{LJ}^{ij}(r_{ij}) = \begin{cases} 4\epsilon_{ij} \left[\left(\frac{\sigma_{ij}}{r_{ij}} \right)^{12} - \left(\frac{\sigma_{ij}}{r_{ij}} \right)^6 \right] & r_{ij} < r_{cut,ij} \\ 0 & r_{ij} \geq r_{cut,ij} \end{cases} \quad (13)$$

where σ_{ij} and ϵ_{ij} are the collision diameter and the well depth of the potential energy for interactions between i and j . The second term in Eq. (12) ($U_{electr}(r)$) is the energy of electrostatic interactions between a pair of molecules which can be written as:

$$U_{electr}(r) = \begin{cases} \frac{1}{4\pi\epsilon_0} \sum_{i=1}^5 \sum_{j=1}^5 \frac{q_i q_j}{r_{ij}} & r < r_{cut,C} \\ 0 & r \geq r_{cut,C} \end{cases} \quad (14)$$

Table 1. The values of the interaction parameters for VPC [44]

| Center | ε/k_B [K] | σ [nm] | q [e] |
|--------|--------------------------|------------------|------------|
| C* | 28.0 | 0.34 | 0 |
| C** | 28.0 | 0.34 | + 0.5 |
| O | 105.8 | 0.296 | - 0.5 |

* Atom of C in the structure.

** Carbonyl group C atom.

where q_i and q_j denote the values of the charges of the centers and ε_0 ($8.8543 \cdot 10^{-12} \text{ C}^2 \text{ J}^{-1} \text{ m}^{-1}$) is the permittivity of the free space. The cut-offs for electrostatic interactions but for all molecules [42] were used and if the centers of the mass of two molecules are located at the distance smaller than the cut-off for electrostatic interactions ($r_{cut,C}$, assumed as equal to 1.5 nm) the sum of the energy of interactions between all pairs of charges occurring in the molecules are calculated, otherwise the electrostatic interactions are neglected. At the cut-off distance the energy of interactions of a pair of molecules is negligibly small (the energy of electrostatic interactions of methane molecules having octopole moments decreases proportionally with the distance in the large power [43]). The values of the parameters of fluid-fluid interactions, taken from [41] are as follows: $\sigma_{CC} = 0.34 \text{ nm}$, $\sigma_{HH} = 0.265 \text{ nm}$, $\sigma_{CH} = 0.3025 \text{ nm}$, $\varepsilon_{CC}/k_B = 55.055 \text{ K}$, $\varepsilon_{HH}/k_B = 7.901 \text{ K}$, $\varepsilon_{CH}/k_B = 30.6 \text{ K}$, $q_C/e = -0.66$, $q_H/e = 0.165$.

The structure of VPC was modeled as the set of Lennard-Jones centres, moreover we take into account the point charges of atoms forming surface carbonyl groups. Generally the equation for the potential energy of adsorbate - adsorbent interactions can be written as:

$$U_{sf} = \sum_{i=1}^{N_C} \sum_{j=1}^5 U_{LJ}^{ij}(r_{ij}) + \sum_{i=1}^{N_K} \sum_{j=1}^2 \sum_{k=1}^5 U_{LJ}^{jk}(r_{ijk}) + \frac{1}{4\pi\varepsilon_0} \sum_{i=1}^{N_K} \sum_{j=1}^2 \sum_{k=1}^5 \frac{q_j q_k}{r_{ijk}} \quad (15)$$

where N_C is the number of (not involved in carbonyl groups) carbon atoms forming the VPC, and N_K is the number of carbonyl groups in the structure. For the last two terms the second summation (with respect to j) denotes the sum with respect to the atoms of carbonyl group ($j = 1$ – carbon atom, $j = 2$ – oxygen atom). For all LJ interactions the cut - offs were placed at $r_{cut,ij} = 5 \sigma_{ij}$. The values of the parameters of interactions for adsorbent were taken from [44] and they are shown in Table 1 (for solid – fluid interactions we used the Lorentz-Berthelot mixing rules).

Table 2. The values of critical parameters, boiling point temperature and density at this point for methane [55]

| | |
|------------------------------|---------|
| T_C [K] | 190.564 |
| p_C [MPa] | 4.5992 |
| T_B [K] | 111.667 |
| d_B [kmol/m ³] | 26.327 |

4. GRAND CANONICAL MONTE CARLO (GCMC) SIMULATIONS

For all above described structures simulations of supercritical methane adsorption at 268, 283 and 298 K using the standard GCMC method were performed [45]. For each adsorption point $25 \cdot 10^6$ iterations were performed (reaching the equilibrium state), and next $25 \cdot 10^6$ equilibrium iterations (from those results the average values were calculated). A single iteration represents an attempt to change the state of a system *via* rotation, displacement, creation or annihilation of the adsorbate (note that the displacement of a molecule in this case is connected with the change in angular position). The probability of an attempt to change the state of a system for rotation and displacement is equal to 1/6, and for creation and annihilation 1/3. Figure 3 shows the recovery of experimental densities of methane by the model applied in this chapter.

5. DESCRIPTION OF SIMULATED ADSORPTION ISOTHERMS

To plot the temperature invariance of the characteristic curve from simulated data it is necessary to recalculate adsorption data and plot them as the volume occupied by methane. We applied the following relation:

$$W(p, T) = \frac{\langle N \rangle(p, T)}{d(T) \cdot N_{Av}} \quad (16)$$

where $\langle N \rangle$ is the average number of methane molecules in the simulation box for a given adsorption point, N_{Av} is the Avogadro number, and d is the density of the adsorbate at a given temperature. It was assumed that the temperature dependence of the latter is given by the formula analogous to Eq.(4):

$$d(T) = d_B \exp[-\alpha(T - T_B)] \quad (17)$$

where d_B is the density of liquid methane at the boiling point (see Tab.2).

To verify the validity of Eqs. (1)-(11) we applied the simultaneous fitting of the branch of isotherms simulated for a given system using the genetic algorithm of Storn and Price [46,47]. This algorithm was successfully applied previously for description of different experimental data [24,26,48], also for description of the isotherm branches [49-52]. The plots of theoretical adsorption isotherms are generated by the DA (Eqs.(1)-(4)), Toth (Eqs. (5),(7),(9),(11)) and Sips equations (Eqs. (6),(8),(10),(11)) and the best fit parameters are: a_0^B , E , n and k (DA equation); a_m^B , $K_{T,0}$, Q_T , $t_{T=268\text{ K}}$ and χ (Toth equation) and a_m^B , $K_{S,0}$, Q_S , $n_{T=268\text{ K}}$ and χ (Sips equation), respectively. The procedure is the same as applied recently [51]. The parameter describing the quality of the fit of theoretical isotherm to simulated one is the determination coefficient:

$$DC_T = 1 - \eta_T \quad (18)$$

where:

$$\eta_T = \frac{\sum_{i=1}^{L_T} (a_{sim,i} - a_{theo,i})^2}{\sum_{i=1}^{L_T} (a_{sim,i} - \bar{a}_{sim})^2} \quad (19)$$

$a_{sim,i}$ and $a_{theo,i}$ are simulated and theoretical adsorption values, respectively, \bar{a}_{sim} is the average adsorption from simulated isotherm, and L_T is the number of points on isotherm at a given temperature. The global parameter describing the quality of the fit is defined by:

$$DC = 1 - \sqrt{\frac{\sum \eta_T^2}{3}} \quad (20)$$

where 3 is the number of temperature values. Tables 3 - 5 shows obtained results.

Table 3. The values of the best-fit parameters obtained using DA equation (Eqs.(1)-(4)) for simulated data

| Structure | a_0^B [molecules/box] | E [kJ/mol] | n | k | DC_T^* | DC |
|--------------------|----------------------------|-----------------|-------|-------|------------------------|--------|
| S0 (S0_000) | 998.7 | 4.754 | 1.280 | 2.717 | 0.9994; 0.9998; 0.9994 | 0.9995 |
| S4 | 993.9 | 5.033 | 1.362 | 2.717 | 0.9992; 0.9997; 0.9993 | 0.9994 |
| S8 | 973.1 | 5.390 | 1.448 | 2.743 | 0.9992; 0.9997; 0.9993 | 0.9993 |
| S12 | 936.3 | 5.775 | 1.519 | 2.802 | 0.9992; 0.9998; 0.9993 | 0.9994 |
| S16 | 888.7 | 6.093 | 1.566 | 2.847 | 0.9993; 0.9998; 0.9994 | 0.9995 |
| S20 | 861.7 | 6.309 | 1.600 | 2.888 | 0.9994; 0.9998; 0.9994 | 0.9995 |
| S24 | 831.2 | 6.499 | 1.620 | 2.932 | 0.9995; 0.9999; 0.9995 | 0.9996 |
| S28 | 804.4 | 6.680 | 1.693 | 2.945 | 0.9995; 0.9999; 0.9996 | 0.9996 |
| S32 | 773.9 | 6.864 | 1.661 | 2.997 | 0.9996; 0.9999; 0.9996 | 0.9996 |
| S35 | 750.2 | 6.992 | 1.688 | 3.037 | 0.9995; 0.9999; 0.9996 | 0.9996 |
| S0_036 | 1010 | 4.855 | 1.296 | 2.717 | 0.9994; 0.9998; 0.9994 | 0.9995 |
| S0_072 | 1021 | 4.945 | 1.310 | 2.717 | 0.9993; 0.9998; 0.9994 | 0.9995 |
| S0_108 | 1031 | 5.078 | 1.337 | 2.732 | 0.9994; 0.9998; 0.9995 | 0.9995 |
| S0_144 | 1039 | 5.194 | 1.357 | 2.754 | 0.9994; 0.9999; 0.9995 | 0.9995 |
| S0_180 | 1051 | 5.313 | 1.375 | 2.799 | 0.9994; 0.9998; 0.9995 | 0.9995 |

*The values arranged according to the rise in temperature.

Table 4. The values of the best-fit parameters obtained using Toth equation (Eqs.(5),(7),(9),(11)) for simulated data

| Structure | a_m^B [molecules/box] | $K_{T,0}$ [1/MPa] | Q_T [kJ/mol] | $t_{T=268\text{ K}}$ | χ | DC_T^* | DC |
|-----------------------|----------------------------|-----------------------|-------------------|----------------------|--------|------------------------------|--------|
| S0 (S0_000) | 2372 | $1.021 \cdot 10^{-3}$ | 12.49 | 0.5210 | 0.3199 | 0.9992; 0.9996; 0.9997 | 0.9995 |
| S4 | 1741 | $1.596 \cdot 10^{-3}$ | 12.00 | 0.6468 | 0.3110 | 0.9991; 0.9994; 0.9996 | 0.9994 |
| S8 | 1458 | $1.803 \cdot 10^{-3}$ | 12.23 | 0.7248 | 0.3261 | 0.9991; 0.9994; 0.9996 | 0.9994 |
| S12 | 1319 | $1.778 \cdot 10^{-3}$ | 12.77 | 0.7351 | 0.3355 | 0.9993; 0.9996; 0.9997 | 0.9995 |
| S16 | 1220 | $1.660 \cdot 10^{-3}$ | 13.36 | 0.7210 | 0.3551 | 0.9994; 0.9996; 0.9997 | 0.9995 |
| S20 | 1162 | $1.671 \cdot 10^{-3}$ | 13.61 | 0.7163 | 0.3453 | 0.9995; 0.9997; 0.9998 | 0.9996 |
| S24 | 1119 | $1.486 \cdot 10^{-3}$ | 14.15 | 0.6936 | 0.3648 | 0.9996; 0.9997; 0.9998 | 0.9997 |
| S28 | 1078 | $1.368 \cdot 10^{-3}$ | 14.62 | 0.6767 | 0.3867 | 0.9996; 0.9998; 0.9998 | 0.9997 |
| S32 | 1031 | $1.265 \cdot 10^{-3}$ | 15.03 | 0.6647 | 0.3899 | 0.9997; 0.9998; 0.9998 | 0.9998 |
| S35 | 983.5 | $1.343 \cdot 10^{-3}$ | 14.99 | 0.6736 | 0.3634 | 0.9997; 0.9998; 0.9999 | 0.9998 |
| S0_036 | 2256 | $1.107 \cdot 10^{-3}$ | 12.54 | 0.5329 | 0.3085 | 0.9992; 0.9995; 0.9997 | 0.9995 |
| S0_072 | 2169 | $1.189 \cdot 10^{-3}$ | 12.57 | 0.5435 | 0.3010 | 0.9992; 0.9995; 0.9997 | 0.9994 |
| S0_108 | 2038 | $1.125 \cdot 10^{-3}$ | 12.94 | 0.5622 | 0.3328 | 0.9992; 0.9995; 0.9997 | 0.9995 |
| S0_144 | 1956 | $1.074 \cdot 10^{-3}$ | 13.24 | 0.5732 | 0.3582 | 0.9992; 0.9996; 0.9997 | 0.9995 |
| S0_180 | 1932 | $1.079 \cdot 10^{-3}$ | 13.40 | 0.5731 | 0.3450 | 0.9993; 0.9995; 0.9997 | 0.9995 |

*The values arranged according to the rise in temperature.

Table 5. The values of the best-fit parameters obtained using Sips equation (Eqs.(6),(8),(10),(11)) for simulated data

| Structure | a_m^B [molecules/box] | $K_{S,0}$ [1/MPa] | Q_S [kJ/mol] | $n_{T=268\text{ K}}$ | χ | DC_T^* | DC |
|------------------------------|----------------------------|-----------------------|-------------------|----------------------|--------|------------------------------|--------|
| S0 (S0_000) | 1705 | $2.897 \cdot 10^{-3}$ | 8.691 | 1.242 | 0.2753 | 0.9996; 0.9998; 0.9999 | 0.9998 |
| S4 | 1496 | $2.911 \cdot 10^{-3}$ | 9.585 | 1.179 | 0.2245 | 0.9995; 0.9997; 0.9998 | 0.9997 |
| S8 | 1345 | $3.048 \cdot 10^{-3}$ | 10.19 | 1.147 | 0.2244 | 0.9995; 0.9997; 0.9998 | 0.9996 |
| S12 | 1233 | $3.027 \cdot 10^{-3}$ | 10.71 | 1.148 | 0.2364 | 0.9996; 0.9998; 0.9999 | 0.9997 |
| S16 | 1141 | $3.013 \cdot 10^{-3}$ | 11.06 | 1.162 | 0.2563 | 0.9997; 0.9998; 0.9999 | 0.9998 |
| S20 | 1087 | $2.951 \cdot 10^{-3}$ | 11.34 | 1.167 | 0.2525 | 0.9998; 0.9999; 0.9999 | 0.9998 |
| S24 | 1041 | $2.851 \cdot 10^{-3}$ | 11.56 | 1.186 | 0.2756 | 0.9998; 0.9999; 0.9999 | 0.9999 |
| S28 | 998.9 | $2.877 \cdot 10^{-3}$ | 11.71 | 1.203 | 0.3007 | 0.9999; 0.9999; 0.9999 | 0.9999 |
| S32 | 953.6 | $2.748 \cdot 10^{-3}$ | 11.96 | 1.215 | 0.3102 | 0.9999; 0.9999; 1.0000 | 0.9999 |
| S35 | 914.6 | $2.624 \cdot 10^{-3}$ | 12.21 | 1.210 | 0.2862 | 0.9999; 1.0000; 1.0000 | 1.0000 |
| S0_036 | 1674 | $2.767 \cdot 10^{-3}$ | 9.009 | 1.241 | 0.2604 | 0.9996; 0.9998; 0.9999 | 0.9998 |
| S0_072 | 1653 | $2.716 \cdot 10^{-3}$ | 9.235 | 1.239 | 0.2488 | 0.9996; 0.9998; 0.9999 | 0.9997 |
| S0_108 | 1611 | $2.767 \cdot 10^{-3}$ | 9.462 | 1.234 | 0.2750 | 0.9996; 0.9998; 0.9999 | 0.9997 |
| S0_144 | 1581 | $2.812 \cdot 10^{-3}$ | 9.629 | 1.231 | 0.2889 | 0.9996; 0.9998; 0.9999 | 0.9997 |
| S0_180 | 1573 | $2.642 \cdot 10^{-3}$ | 9.895 | 1.236 | 0.2823 | 0.9996; 0.9998; 0.9999 | 0.9998 |

*The values arranged according to the rise in temperature.

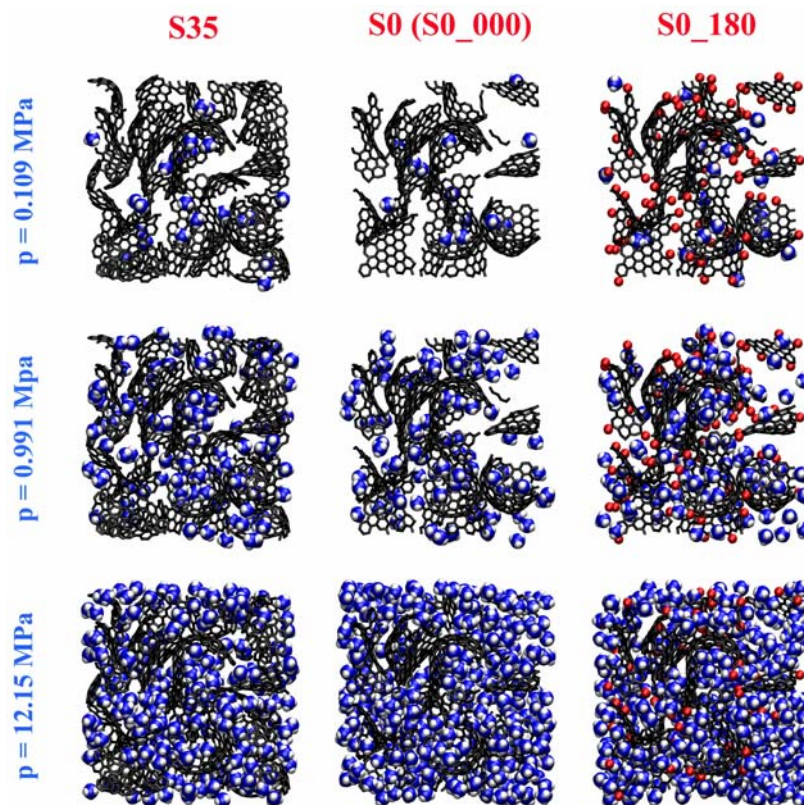


Figure 4. Snapshots of equilibrated methane – VPC systems ($T = 283$ K) for arbitrarily chosen pressures (the view from the top of simulation boxes after dividing them into two equal parts by the xy plane).

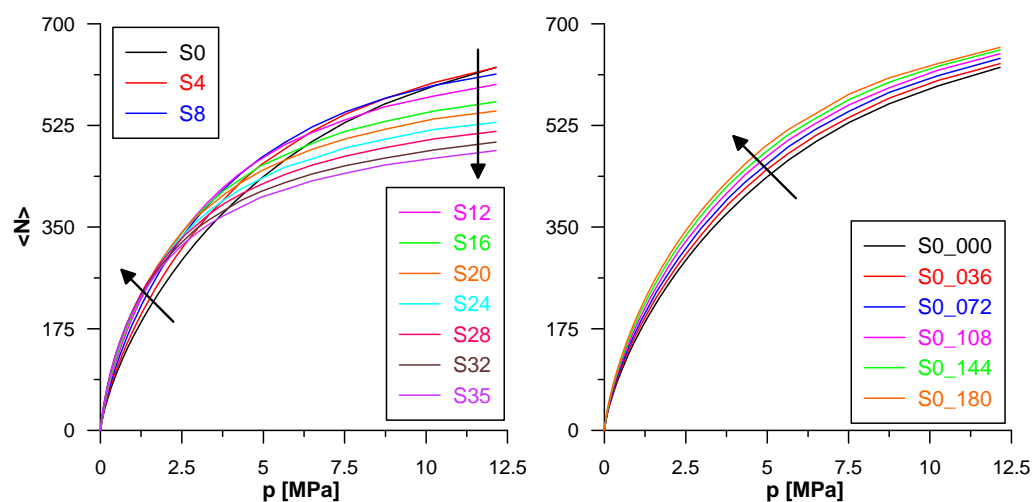


Figure 5. (Continued)

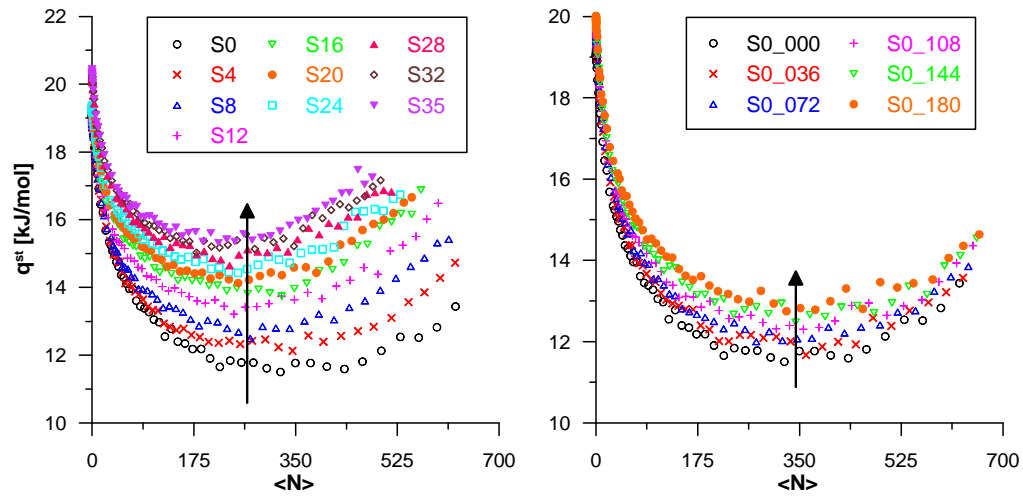


Figure 5. The comparison of the plots of simulated adsorption isotherms of methane at 283 K and the plots of related adsorption enthalpy (calculated from the theory of fluctuations). Isotherms are presented as the average number of molecules in the simulation box ($\langle N \rangle$). The arrows show the changes from S0 up to S35 and from S0_000 up to S0_180.

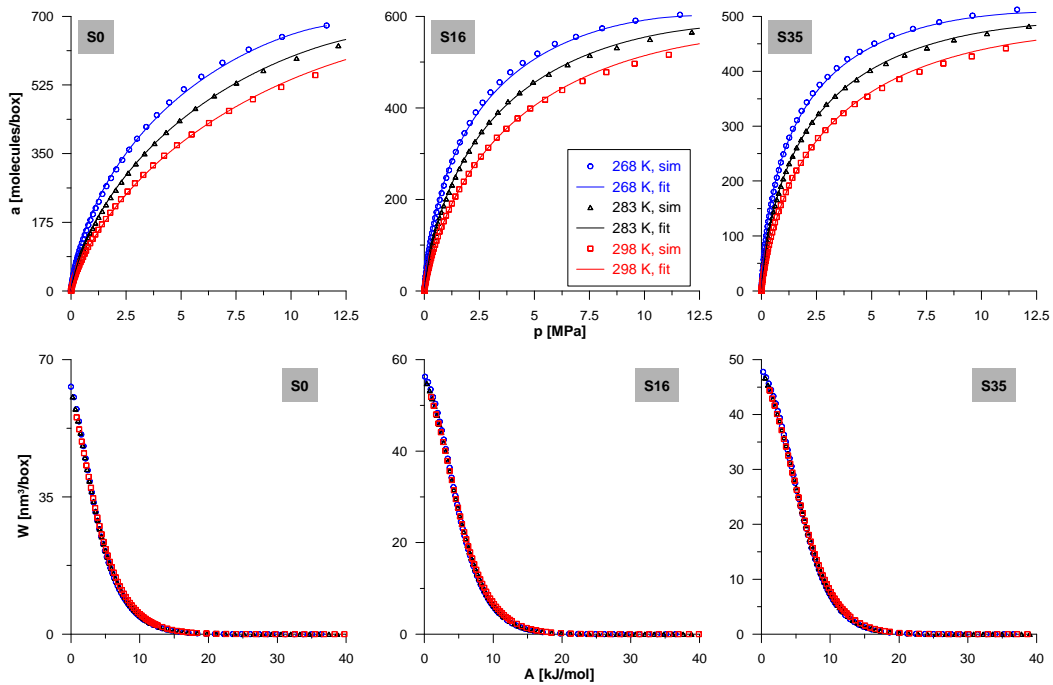


Figure 6. The results of fitting of DA equation (Eqs.(1)-(4)) to simulated data for arbitrarily chosen systems with gradually changed porosity (upper panel) and the characteristic curves generated for the same systems basing on simulated data.

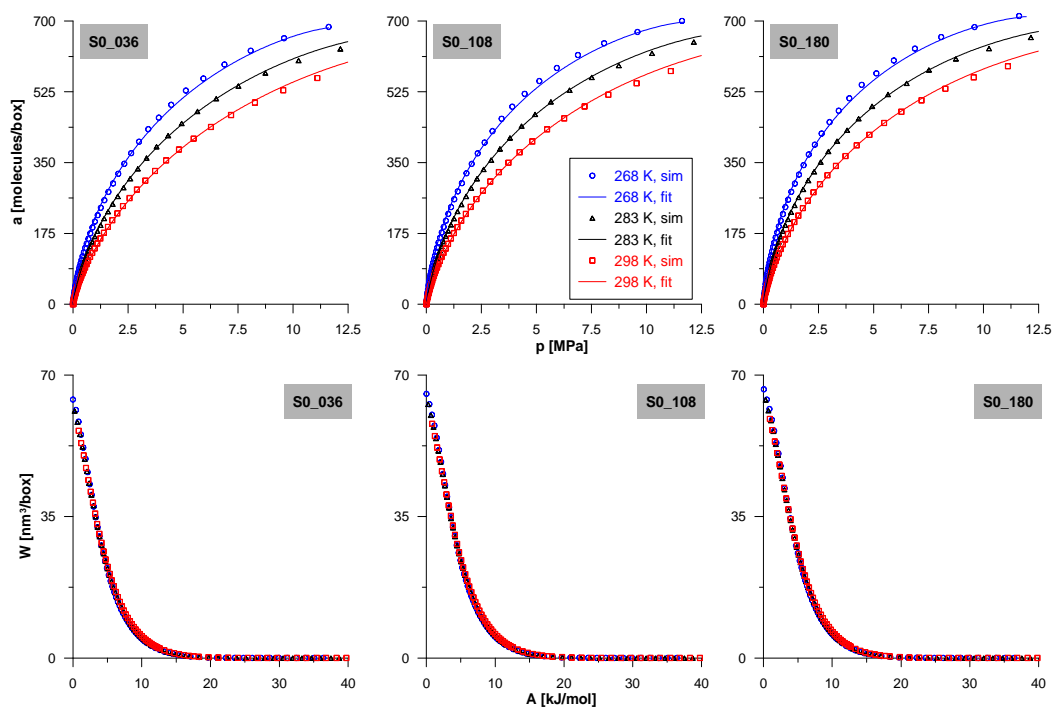


Figure 7. The same as in Figure 4 but for systems with gradually changed number of surface carbonyls.

6. RESULTS AND DISCUSSION

From the results shown in Figure 2 one can conclude that proposed procedures of creation of VPCs lead to satisfactory results. In fact the series of carbons with progressively changed porosity (PSD shifts from S0 up to S35 towards smaller average pore diameters) were obtained. On the other hand virtual oxidation retains porosity almost unchanged but the chemical composition of surface is strongly influenced by introduction of surface carbonyl groups (small differences in porosity are due to steric effects caused by surface groups). From Figure 3 one can conclude satisfactory recovering of experimental density of methane in the range applied for simulations of high pressure isotherms, and this is the confirmation of validity of applied parameters of intermolecular methane-methane interactions. In Figure 4 selected snapshots from GCMC isotherms for two of studied structures are shown, and the isotherms (and isosteric enthalpy) are plotted in Figure 5. One can observe the rise in adsorption in the range up to c.a. 3 MPa with the decrease in the average pore diameter of VPC (higher methane compression) however at larger pressures the steric effect dominates. Interesting are also the results showing that the virtual oxidation leads to the rise in methane adsorption, therefore it can be postulated that the mild oxidation of carbon (i.e. remaining carbon skeleton intact) with creation of carbonyl groups should lead to rise in methane adsorption. One can observe a progressive rise in the enthalpy of adsorption with the decrease in average pore diameter (due to the rise in the van der Waals energy) and with the rise in the number of surface carbonyls, however in the latter case this rise is smaller due to small electric moment of methane molecule. Table 3 shows the results of fitting of DA model to

simulated data by the above described procedure (some representative cases are also shown in Figures 6 and 7). The correlations plotted in Figure 8 confirm that even in realistic carbon model the optimal pore diameter for methane adsorption is located around 0.8 nm and this is similar diameter as obtained from simulations in slit-like pores. One can also observe mentioned above rise in adsorption with the rise in content of surface carbonyls. The most important results are plotted in Figure 9. The inverse relation between characteristic energy of methane adsorption and pore diameter confirms the well known observation that E is related to the pore diameter [26,53,54]. For the studied systems also the parameter n of the DA model is correlated with the micropore diameter i.e. the more heterogeneous is carbon structure the larger n value is. The values of the parameter k obtained from fitting of the GCMC results by Eqs. (1)-(4) are for some systems close to the upper limit reported by Amankwah and Schwarz [32]. For this parameter one can also observe systematic changes with carbon porosity. For the systems: S0, S4, S0_036 and S0_072 the values of this parameter being the lowest possible for acceptance (to conserve the physical sense) were obtained. This is due to the fact that the smaller value of this parameter must predict the value of p_s^* (Eqs. (1)-(4)) being not smaller than the largest pressure observed on isotherm therefore, for mentioned systems, the value of k is related at 268 K to the p_s^* equal to the largest pressure on isotherm for temperature. If one omits those points in Figure 9 (marked as crosses) a linear relation occurs between k and the average pore diameter. From Figure 10 one can observe that E , n as well as k are also correlated with the contents of oxygen in structure.

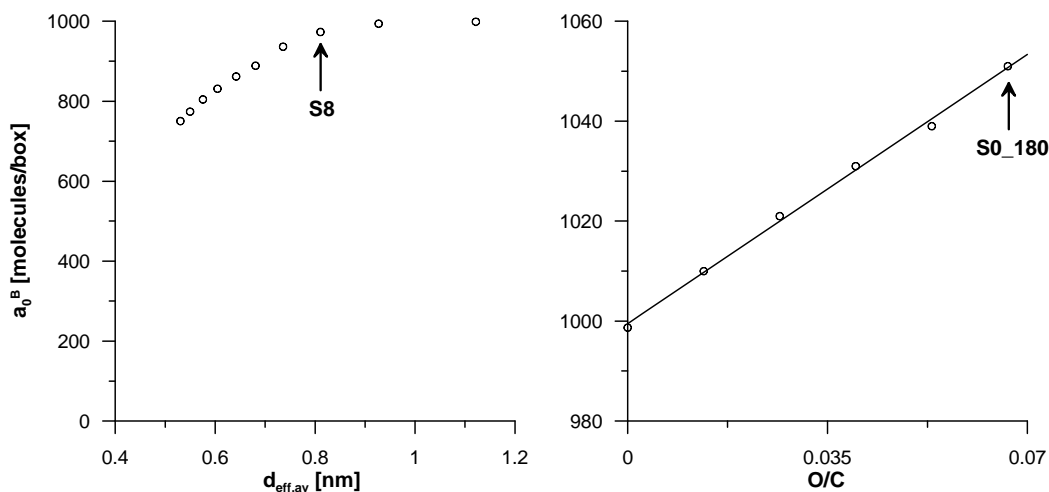


Figure 8. The relation between maximum methane adsorption at the boiling temperature (calculated from the fitting of DA equation (Eq.(1)-(4)) to simulated isotherms) and the pore diameter from BG model (left) and the ratio of oxygen to carbon in VPC (right).

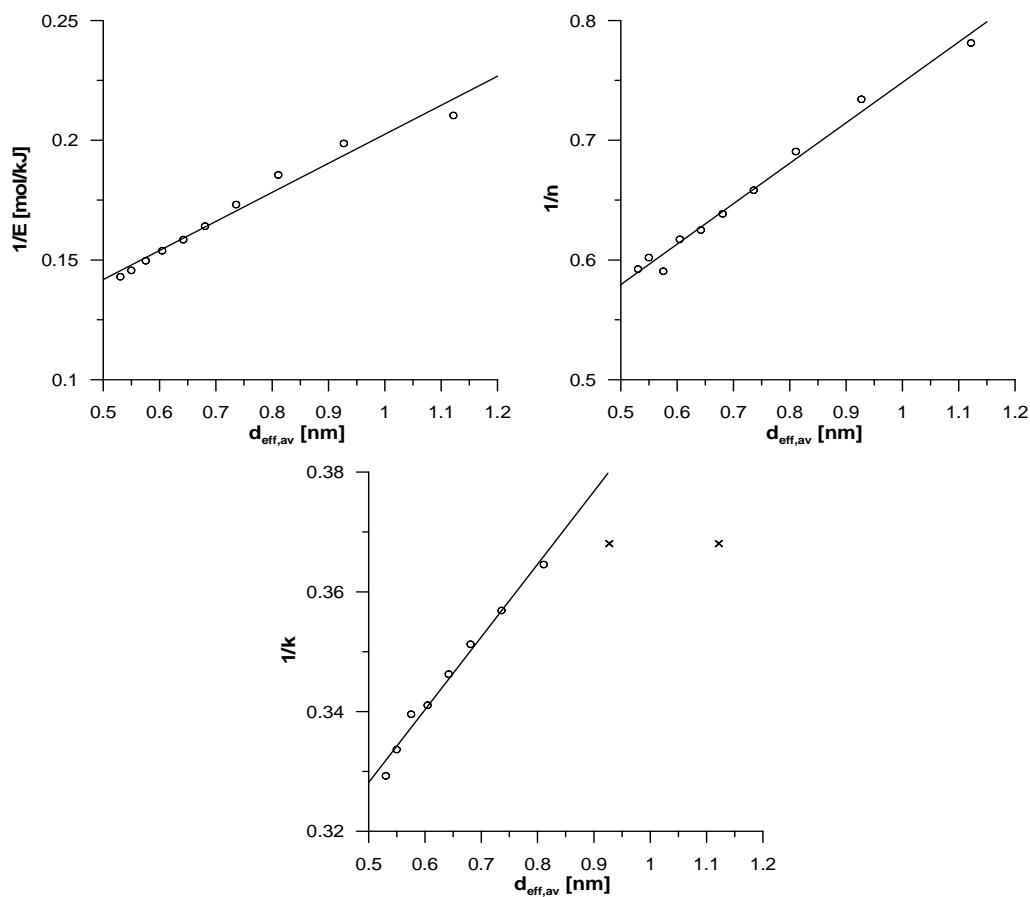


Figure 9. The correlation between average diameters of pores from BG method and the best fit parameters of Eqs.(1)-(4) for the series of VPCs with different porosity (S0 – S35). In the case of parameter k we excluded from linear regression those systems where the k value reaches the lowest physical range (points marked as crosses).

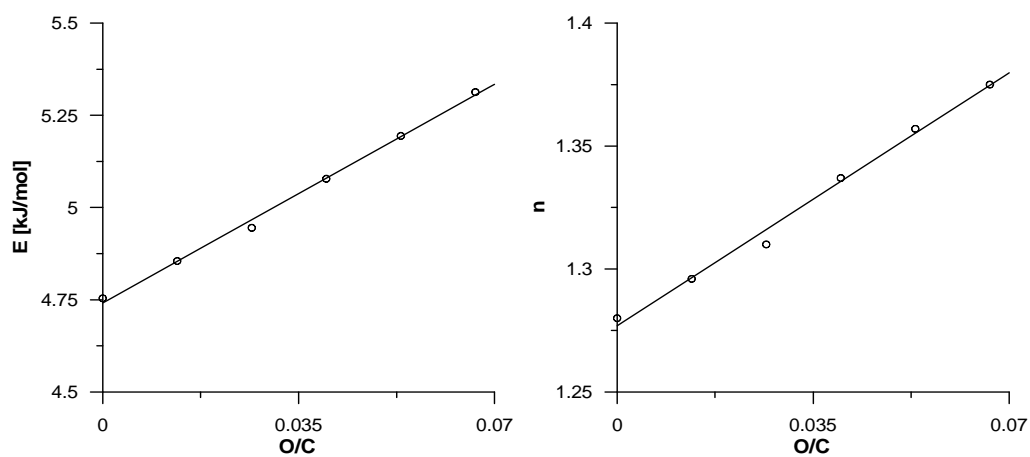


Figure 10. (Continued)

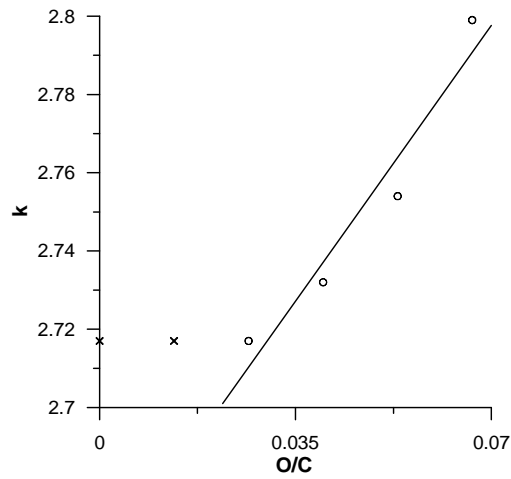


Figure 10. The correlations between the ratio of oxygen to carbon in VPCs and the parameters of Eqs.(1)-(4) for the structures with different contents of surface carbonyl groups (S0_000 – S0_180). In the case of parameter k we excluded from linear regression those systems where the k value reaches the lowest physical range (points marked as crosses).

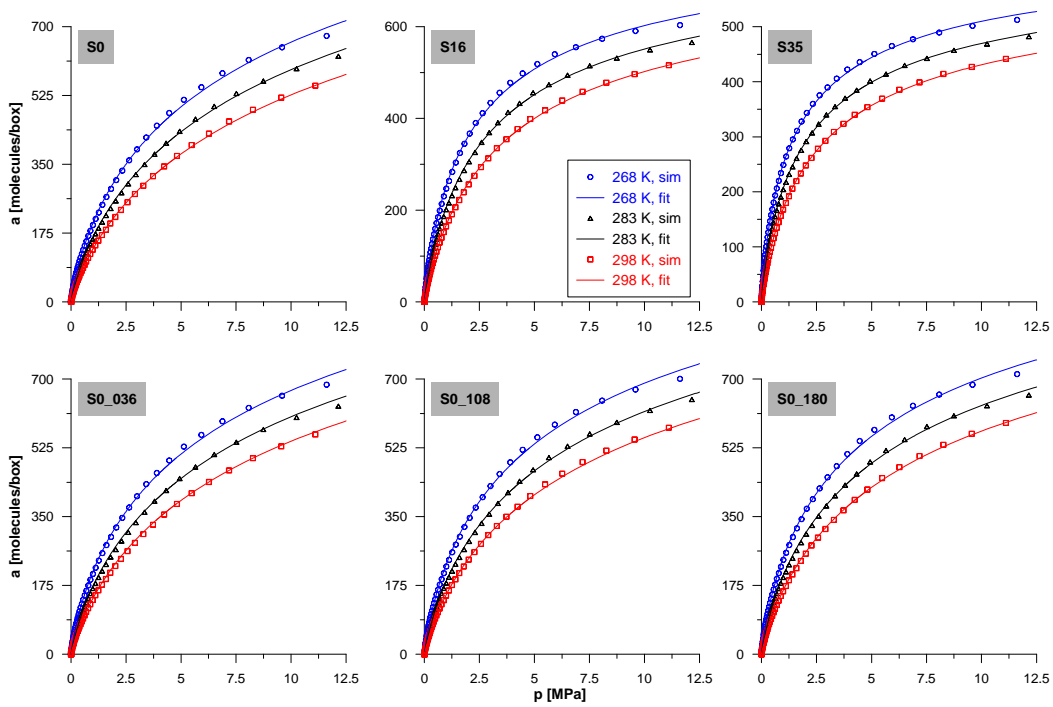


Figure 11. The results of fitting of Toth equation (Eqs. (5),(7),(9),(11)) to isotherms simulated for arbitrary chosen systems.

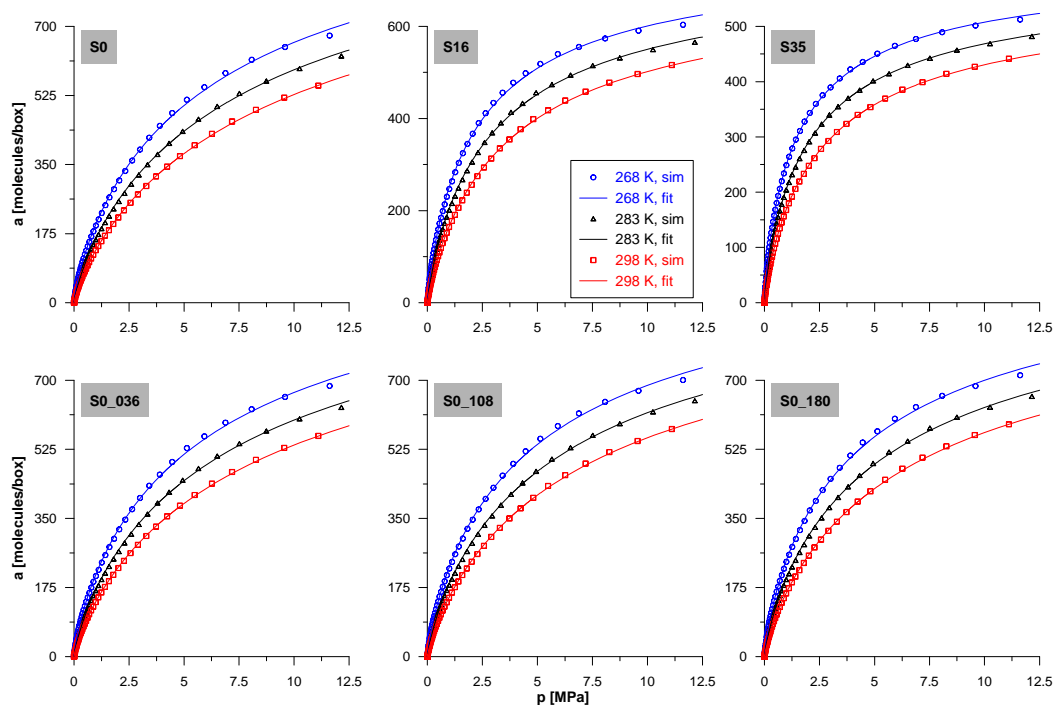


Figure 12. The results of fitting of Sips equation (Eqs. (6),(8),(10),(11)) to isotherms simulated for arbitrary chosen systems.

The description of simulated data by Toth and Sips models (Eqs.(5) and (6)) leads to slightly better fit comparing to this from DA model (see Tabs. 4 and 5) however, the differences in the quality of the fit are rather small. Figures 11 and 12 show the results of fitting for arbitrary chosen systems. The values of the parameter Q_T of the Toth equation (equal to the isosteric heat at the zero coverage [40], Tab.4) and Q_S in the Sips equation (equal to the isosteric heat at the fractional loading 0.5 [40], Tab.5) quite well correlate with the values calculated from the GCMC simulations (shown in Figure 5) showing similar tendency with the rise in microporosity as well as with the rise in oxygen content. The constant of the both models are related to the effective micropore diameters calculated from the BG method (see Figure 13). In this case the logarithm of the constant K_T linearly decreases from structure S35 up to S8. However, for the next two remaining structures this decrease is not so sharp. In contrast the linear correlation between $\log K_S$ and effective pore diameter is observed for all studied VPCs. This is due to mentioned above differences between the meaning of Q_T and Q_S (therefore related differences between the constants of the both equations). Figure 13 also shows that for oxidised carbons the constants of the both equations linearly increase with the content of oxygen on surface. As mentioned above, the constant t of the Toth model is related to the heterogeneity for the adsorbate – adsorbent pair. Therefore, with the rise in the number of surface oxygen groups in the system one can expect the larger surface heterogeneity of the system, since porosity is constant. In fact Figure 14 confirms this expectation since almost linear correlation between the values of t and oxygen content occurs.

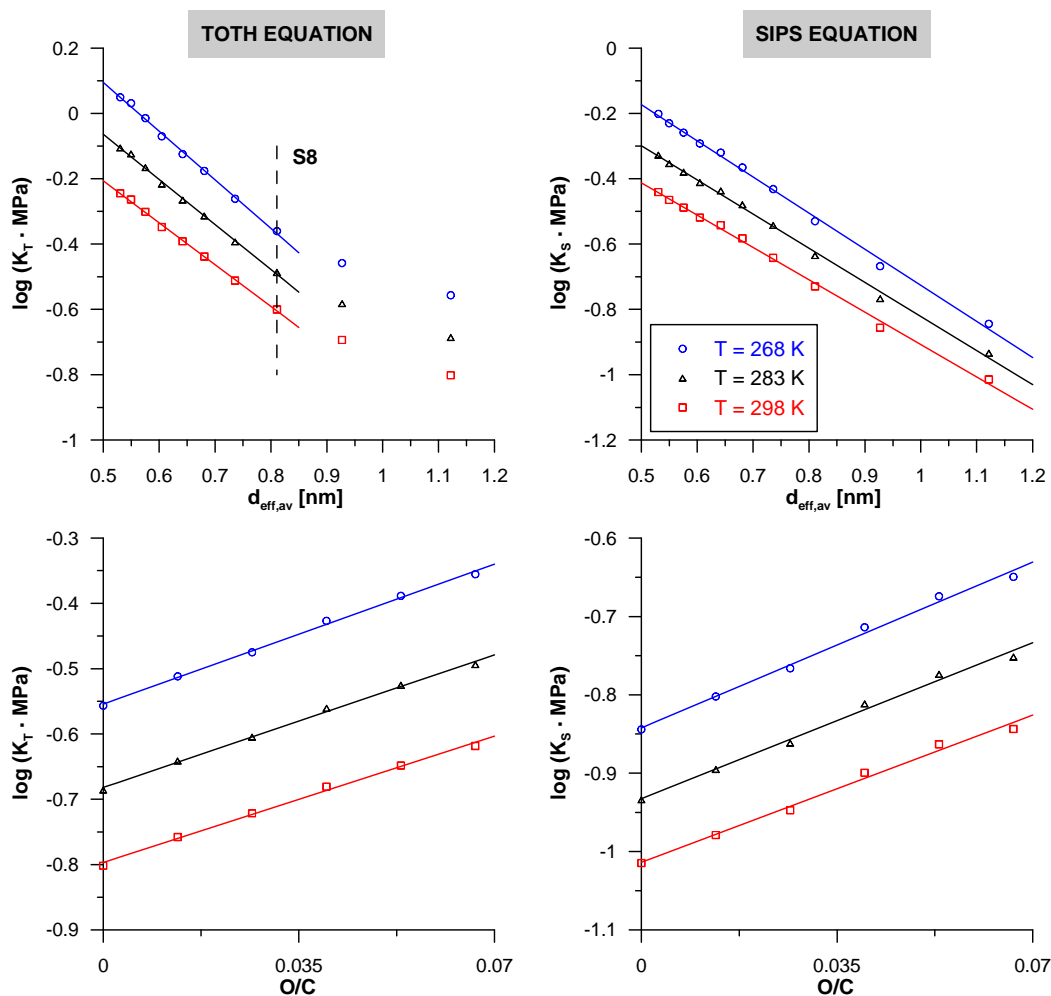


Figure 13. The correlation between constants of Toth and Sips equations (K_T and K_S , calculated using Eqs. (7) and (8) and the values tabulated in Tabs. 4 and 5) and the pore diameters from BG method (for the series with different porosity) and the content of oxygen (for the structures with different amount of carbonyl groups).

7. CONCLUSION

In a realistic carbon model the optimal pore diameter for methane adsorption is similar as for slit-like carbon micropores (i.e. around 0.8 nm). Dubinin-Astakhov model describes simulated isotherms satisfactorily. The validity of relation proposed by Amankwah and Schwarz [32] for determination of the apparent saturated vapour pressure of supercritical methane was confirmed, and the proposed VPC model leads to realistic (i.e. similar to obtained in experiment) values of the parameter k . Mild oxidation of carbons leading to creation of surface carbonyl groups increases methane adsorption. The parameters of the DA model as well as k are linearly correlated with the pore diameters and the contents of surface oxygen groups, however those correlations need further experimental confirmation. The

empirical Toth and Sips adsorption isotherm equations also describe simulated methane data well and even small rise in the value of DC is observed. The constants of the both equations correlate with the pore diameters and oxygen content in virtual porous carbons. Heterogeneity parameter t of the Toth model shows almost linear increase with the number of oxygen surface groups in the carbon structure.

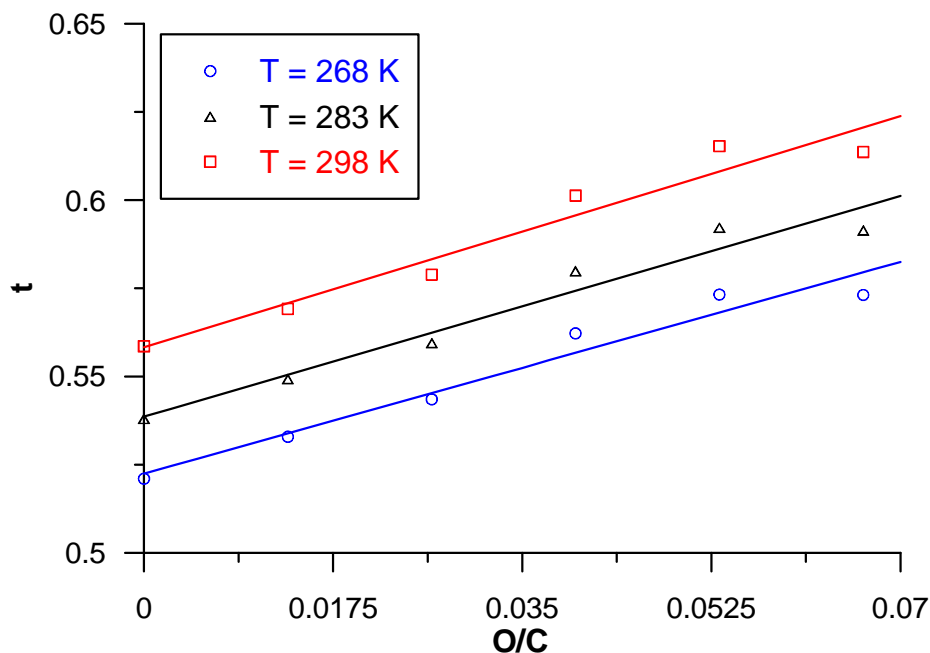


Figure 14. The correlation between the value of t constant of Toth equation (Eq.(9)) and the content of oxygen in oxidised structure.

ACKNOWLEDGEMENTS

We thank the editors for invitation. The authors acknowledge the use of the computer cluster at Poznań Supercomputing and Networking Center and the Information and Communication Technology Center of the Nicolaus Copernicus University (Toruń, Poland). The project was supported by grants: N N204 009934 and N N204 288634. This paper was supported by the Foundation for Polish Science (S.F.).

REFERENCES

- [1] Lozano-Castello, D.; Cazorla-Amoros, D.; Linares-Solano, A. *Energy Fuels* 2002, 16, 1321-1328.
- [2] Celzard, A.; Fierro, V. *Energy Fuels* 2005, 19, 573-583.
- [3] Guan, C.; Su, F.; Zhao, X.S.; Wang, K. *Sep. Purif. Technol.* 2008, 64, 124-126.
- [4] Bae, J.-S.; Bhatia, S. K. *Energy Fuels* 2006, 20, 2599-2607.

-
- [5] Wang, S. *Energy Fuels* 2007, 21, 953-956.
- [6] Muto, A.; Bhaskar, T.; Tsuneishi, S.; Sakata, Y.; Ogasa, H. *Energy Fuels* 2005, 19, 251-257.
- [7] Dai, X. D.; Liu, X. M.; Qian, L.; Qiao, K.; Yan, Z. F. *Energy Fuels* 2008, 22, 3420-3423.
- [8] Zhou, Y.; Wang, Y.; Chen, H.; Zhou, L. *Carbon* 2005, 43, 2007-2012.
- [9] Urabe, Y.; Ishikura, T.; Kaneko, K. *J. Colloid Interface Sci.* 2008, 319, 381-383.
- [10] Sosin, K. A.; Quinn, D. F. *J. Porous Mater.* 1995, 1, 111-119.
- [11] Chen, X. S.; McEnaney, B.; Mays, T. J.; Alcaniz-Monge, J.; Cazorla-Amoros, D.; Linares-Solano, A. *Carbon* 1997, 35, 1251-1258.
- [12] Inagaki, M. *New Carbons, Control of Structure and Functions*; Elsevier: Amsterdam, 2000.
- [13] McGreevy, R. L.; Pusztai, L. *Mol. Simul.* 1988, 1, 359-367.
- [14] Thomson, K. T.; Gubbins, K. E. *Langmuir* 2000, 16, 5761-5773.
- [15] Petersen, T.; Yarovsky, I.; Snook, I.; McCulloch, D. G.; Opleteal, G. *Carbon*, 2003, 41, 2403-2411.
- [16] Pikunic, J.; Clinard, C.; Cohaut, N.; Gubbins, K. E.; Guet, J.-M.; Pellenq, R.J.-M.; Rannou I.; Rouzaud, J.-N. *Langmuir* 2003, 19, 8565-8582.
- [17] J Brennan, K.; Thomson, K. T.; Gubbins, K. E. *Langmuir* 2002, 18, 5438-5447.
- [18] Harris, P. J. F.; Tsang, S. C. *Philos. Mag. A* 1997, 76, 667-677
- [19] Harris, P. J. F. *Int. Mater. Rev.* 1997, 42, 206-218.
- [20] Harris, P. J. F.; Burian A.; Duber, S. *Philos. Mag. Lett.* 2000, 80, 381-386.
- [21] Harris, P. J. F. *Crit. Rev. Solid State Mat. Sci.* 2005, 30, 235-253.
- [22] Harris, P. J. F.; Liu, Z.; Suenaga, K. *J. Phys. Condens. Mat.* 2008, 20, 362201.
- [23] Harris, P. J. F. In *Carbon Materials Theory and Practice*; Terzyk, A. P.; Gauden, P. A.; Kowalczyk, P.; Eds., Research Signpost: Kerala, 2008; pp 1-14.
- [24] Terzyk, A. P.; Furmaniak, S.; Gauden, P. A.; Harris, P. J. F.; Włoch, J.; Kowalczyk, P. *J. Phys. Condens. Mat.* 2007, 19, 406208.
- [25] Terzyk, A. P.; Furmaniak, S.; Harris, P. J. F.; Gauden, P. A.; Włoch, J.; Kowalczyk, P.; Rychlicki, G. *Phys. Chem. Chem. Phys.* 2007, 9, 5919-5929.
- [26] Terzyk, A. P.; Furmaniak, S.; Gauden, P. A.; Harris, P. J. F.; Włoch, J. *J. Phys. Condens. Mat.* 2008, 20, 385212.
- [27] Furmaniak, S.; Terzyk, A. P.; Gauden, P. A.; Harris, P. J. F.; Kowalczyk, P. *J. Phys. Condens. Mat.* 2009, 21, 315005.
- [28] Bhattacharya, S.; Gubbins, K. E. *Langmuir* 2006, 22, 7726-7731.
- [29] Dubinin, M. M.; Astakhov, A. V. *Izv. AN SSSR Ser. Khim.* 1971, 1, 5-24 (in Russian).
- [30] Dubinin, M. M. *Adsorption and Porosity*; Warsaw: WAT, 1975 (in Polish).
- [31] Li, M.; Gu, A. Z. *J. Colloid Interface Sci.* 2004, 273, 356-361.
- [32] Amankwah, K. A. G.; Schwarz J. A. *Carbon* 1995, 33, 1313-1319.
- [33] Dubinin, M. M. *Chem. Rev.* 1960, 60, 235-241.
- [34] Ozawa, S.; Kusumi, S.; Ogino, Y. *J. Colloid Interface Sci.* 1976, 56, 83-91.
- [35] Choi, B.-U; Choi, D.-K.; Lee, Y.-W.; Lee, B.-K.; Kim, S.-H. *J. Chem. Eng. Data* 2003, 48, 603-607.
- [36] Himeno, S.; Komatsu, T.; Fujita, S. *J. Chem. Eng. Data* 2005, 50, 369-376.
- [37] Lee, J.-W.; Kang, H.-C.; Shim, W.-G.; Kim, C.; Moon, H. *J. Chem. Eng. Data* 2006, 51, 963-967.

-
- [38] Lee, J.-W.; Balathanigaimani, M.S.; Kang, H.-C.; Shim, W.-G.; Kim, C., Moon, H. *J. Chem. Eng. Data* 2007, 52, 66-70.
- [39] Rarзад, S.; Taghikhani, V.; Ghotbi, C.; Aminshahidi, B.; Nemat Lay, E. *J. Nat. Gas Chem.* 2007, 16, 22-30.
- [40] Do, D.D. *Adsorption Analysis: Equilibria and Kinetics*; London: Imperial College Press, 1998.
- [41] Terzyk, A. P.; Furmaniak, S.; Gauden, P. A.; Kowalczyk, P. *Adsorpt. Sci. Technol.* 2009, 27, 281-296.
- [42] Ungerer, P.; Tavitian, B.; Boutin, A. *Applications of Molecular Simulation in the Oil and Gas Industry*; Edition Technip: Paris, 2005.
- [43] Gray, C. G.; Gubbins, K. E. *Theory of Molecular Fluids*; Clarendon Press: Oxford, 1984, Vol. 1.
- [44] Jorge, M., Schumacher, C.; Seaton, N. A. *Langmuir* 2002, 18, 9296-9306.
- [45] Frenkel, D.; Smit, B. *Understanding Molecular Simulation*; Academic Press: San Diego, 1996.
- [46] Storn, R.; Price, K. In *Proceedings of 1996 IEEE International Conference on Evolutionary Computation (ICEC '96)*. Nagoya University, 1996 pp 842-844.
- [47] Storn, R.; Price, K. *J. Global Optim.* 1997, 11, 341-359.
- [48] Furmaniak, S.; Gauden, P. A.; Terzyk, A. P.; Rychlicki, G. *Adv. Colloid Interface Sci.* 2008, 137, 82-143.
- [49] Furmaniak, S.; Terzyk, A. P.; Gauden, P. A.; Rychlicki, G. *J. Food Eng.* 2007, 79, 718-723.
- [50] Furmaniak, S.; Terzyk, A. P.; Gauden, P. A. *J. Food Eng.* 2007, 82, 528-535.
- [51] Furmaniak, S.; Terzyk, A. P.; Czepirski, L.; Komorowska-Czepirska, E.; Szymońska, J.; Gauden, P. A. In *Focus on Food Engineering Research and Developments*; Pletney V. N.; ed.; Nova Science Publishers: New York, 2007; pp 497-515.
- [52] Furmaniak, S.; Terzyk, A. P.; Czepirski, L.; Komorowska-Czepirska, E.; Szymońska, J.; Gauden, P. A. *Food* 2009, 3, 13-17.
- [53] Chen, S. G.; Yang, R. T. *J. Colloid Interface Sci.* 1996, 177, 298-306.
- [54] Chen, S. G.; Yang, R. T. *Langmuir* 1994, 10, 4244-4249.
- [55] NIST Standard Reference Database Number 69. <http://webbook.nist.gov/chemistry/>